Molecular Genetics and Metabolism Reports 33 (2022) 100919

Contents lists available at ScienceDirect

Molecular Genetics and Metabolism Reports

journal homepage: www.elsevier.com/locate/ymgmr

Dysregulated DNA methylation in the pathogenesis of Fabry disease

Jin-Song Shen [a,*], Uthra Balaji [b], Kunitoshi Shigeyasu [c], Yoshinaga Okugawa [c], Siamak Jabbarzadeh-Tabrizi [a], Taniqua S. Day [a], Erland Arning [a], John Marshall [d], Seng H. Cheng [d], Jinghua Gu [b], Raphael Schiffmann [a], Teodoro Bottiglieri [a], Ajay Goel [c]

[a] Institute of Metabolic Disease, Baylor Scott & White Research Institute, 3434 Live Oak Street, Dallas, TX 75024, United States of America
[b] Baylor Scott & White Research Institute, Biostatistics, Dallas, TX, United States of America
[c] Center for Gastrointestinal Research; Center for Epigenetics, Cancer Prevention and Cancer Genomics, Baylor Research Institute, Dallas, TX, United States of America
[d] Sanofi Genzyme, 49 New York Avenue, Framingham, MA 01701, United States of America

ARTICLE INFO

Keywords:
Fabry disease
α-Galactosidase A
Globotriaosylceramide
DNA methylation
Deoxygalactonojirimycin
Substrate reduction therapy

ABSTRACT

Fabry disease is an X-linked lysosomal storage disorder caused by a deficiency of α-galactosidase A and subsequent accumulation of glycosphingolipids with terminal α-D-galactosyl residues. The molecular process through which this abnormal metabolism of glycosphingolipids causes multisystem dysfunction in Fabry disease is not fully understood. We sought to determine whether dysregulated DNA methylation plays a role in the development of this disease. In the present study, using isogenic cellular models derived from Fabry patient endothelial cells, we tested whether manipulation of α-galactosidase A activity and glycosphingolipid metabolism affects DNA methylation. Bisulfite pyrosequencing revealed that changes in α-galactosidase A activity were associated with significantly altered DNA methylation in the androgen receptor promoter, and this effect was highly CpG loci-specific. Methylation array studies showed that α-galactosidase A activity and glycosphingolipid levels were associated with differential methylation of numerous CpG sites throughout the genome. We identified 15 signaling pathways that may be susceptible to methylation alterations in Fabry disease. By incorporating RNA sequencing data, we identified 21 genes that have both differential mRNA expression and methylation. Upregulated expression of collagen type IV alpha 1 and alpha 2 genes correlated with decreased methylation of these two genes. Methionine levels were elevated in Fabry patient cells and Fabry mouse tissues, suggesting that a perturbed methionine cycle contributes to the observed dysregulated methylation patterns. In conclusion, this study provides evidence that α-galactosidase A deficiency and glycosphingolipid storage may affect DNA methylation homeostasis and highlights the importance of epigenetics in the pathogenesis of Fabry disease and, possibly, of other lysosomal storage disorders.

1. Introduction

Fabry disease is an X-linked lysosomal storage disorder (LSD) caused by deficient activity of α-galactosidase A (α-gal A) [1]. This enzyme deficiency results in an inability of the cells to catabolize glycosphingolipids (GSLs) with terminal α-D-galactosyl residues, mainly globotriaosylceramide (Gb_3). GSLs accumulation occurs in the lysosomes of almost all cell types; however, it is particularly prominent in vascular endothelial and smooth muscle cells [2]. Major clinical manifestations include neuropathic pain, progressive renal insufficiency, cardiac disease and strokes. Male patients typically present with the most severe form of the disease [3]. Clinical abnormalities in heterozygous female patients are generally milder, but can occasionally be as severe as those observed in classically affected male patients.

A number of genes have been reported to be abnormally expressed in Fabry patients and a mouse model of the disease [4–9], which may contribute to the pathogenesis of the disease. However, the molecular mechanism by which α-gal A deficiency causes the noted aberrant gene expression remains unclear.

DNA methylation represents one of the most important epigenetic mechanisms for gene regulation. Aberrant DNA methylation has been implicated in cancers, neurodegenerative and autoimmune disorders [10]. However, the association between DNA methylation and Fabry disease and other LSDs is largely unknown. Echevarria et al. [11] analyzed X-chromosome inactivation (XCI) in 56 female Fabry patients, and found that most patients had random inactivation and that, in

* Corresponding author at: 4D Molecular Therapeutics, 5858 Horton St., Suite 455, Emeryville, CA 94608, United States of America.
E-mail address: Jinsong.shen@gmail.com (J.-S. Shen).

https://doi.org/10.1016/j.ymgmr.2022.100919
Received 29 August 2022; Accepted 21 September 2022

patients with skewed XCI (29%), disease progression was correlated with the direction of skewing. Rossanti et al. [12] reported that skewed XCI resulting in predominant inactivation of the normal allele was observed only in one out 9 females patients with Fabry disease that were analyzed. Recently, De Riso et al. [13] studied XCI process using epiallele distribution analysis approach, and demonstrated substantial concordance in direction of the methylation imbalance between androgen receptor (AR) and *GLA* genes. Hossain et al. [14,15] directly analyzed methylation of the *GLA* gene in female Fabry patients, and showed that methylation of the non-mutated allele correlated with disease severity. These studies highlighted the potential effect of methylation of *GLA* gene on α-gal A activity and disease phenotype in heterozygous females (for a review on the role of DNA methylation in Fabry disease, see Di Risi et al. [16]). However, the role of epigenetic modifications as a downstream mediator in disease pathogenesis has not been studied. We hypothesized that Fabry disease affects DNA methylation homeostasis, which might contribute to dysregulated gene expression and development of the disease. In this study, we investigated whether α-gal A deficiency and abnormal GSL metabolism cause aberrant DNA methylation.

2. Materials and methods

2.1. Cell culture and treatments

IMFE1 (a microvascular endothelial cell line established from a skin biopsy of a male Fabry patient) [17] and its derivatives were cultured in EGM-2MV medium (Lonza). IMFE1(α-gal+) and IMFE1(mock) cells were generated by stably transducing IMFE1 cells with a retroviral vector encoding normal α-gal A cDNA or an 'empty' control retrovirus, respectively [6]. IMFE1(α-gal+) and IMFE1(mock) cells were maintained in parallel to avoid passage-related variations between the 2 cell lines. Both cell lines used in this study had been passaged 9 times post-infection with α-gal A-expressing retrovirus or control vector, which is equivalent to at least 15 population doublings. Cell morphology and growth rate of this pair of cells were indistinguishable.

For the short-term treatment experiment, IMFE1 parental cells were treated with either 500 μM 1-deoxygalactonojirimycin (DGJ) or 0.5 μM GZ161 [18] for 12 days. The culture media were changed every 2–3 days with media containing freshly added compounds. Mock-treated control cells were cultured in parallel, and PBS was used in place of the DGJ or GZ161. There was no detectable cytotoxicity in drug-treated cells. Cell morphology and growth rates were indistinguishable in sham-, DGJ- and GZ161-treated groups. During the treatment, cells grew actively and underwent 4–5 population doublings.

2.2. Mouse tissues

Kidneys were obtained from 6-month-old male Fabry and WT mice. Both colonies had mixed genetic backgrounds of C57BL/6 and 129 strains (~75% C57BL/6 background) as described previously [6]. Animal procedures were reviewed and approved by the Institutional Animal Care and Use Committee of Baylor Scott & White Research Institute.

2.3. Gb_3 immunostaining and quantitative analysis

Gb_3 immunofluorescence staining was performed using a Gb_3–specific mouse monoclonal antibody as previously described [6]. Quantitative measurement of Gb_3 levels was performed using mass spectrometry as described [6].

2.4. Bisulfite treatment and pyrosequencing

Genomic DNA was extracted using Qiagen DNeasy kit. Bisulfite treatment was performed using EZ DNA Methylation-Gold kit (Zymo Research) with 300 ng genomic DNA as starting material. Pyrosequencing was performed using PyroMark Q96 MD (Qiagen) according to manufacturer's instructions. Primers used were: AR CpG hot spot 1 (forward, Biotin-AGGAAGTAGGGGTTTTTTAGGGT; reverse, TCCCCTTTCCTTTTCTCCC; sequencing, TCTCCCCTCCCCTCA; amplicon 132 bp); AR CpG hot spot 2 (forward, GGGGAGTTAGTTTGTTGGGAGAG; reverse, Biotin-CAATCCTACCAAACACTTTCCTTACTT; sequencing, GAGTTAGTTTGTTGGGAGA; amplicon 276 bp).

2.5. DNA methylation array

Data from Infinium Methylation EPIC array that covers 865,859 CpG sites was assessed for quality using Genome Studio software (detected CpGs, bisulfite conversion controls, hybridization controls). The raw data (IDAT files) that contains intensity signals was read into R using functions from minfi package [19]. MethylationEPIC_v-1-0_B4 manifest was used to annotate the probes from EPIC array using IlluminaHumanMethylationEPICanno.ilm10b4.hg19 package [20]. Probe filtering was performed to remove CpG sites that have low detection *p*-value, known SNPs and cross-reactive probes. After quality control filtering, 793,793 sites with reliable methylation data were used for further analysis. Intensity values were normalized using control probes to generate β and M-values. Normalized M-values were used to identify differentially methylated probes using the limma package [21]. Differentially methylated regions were analyzed using the DMRcate package [22].

Principal component analysis showed that samples in each group ($n = 3$ per group) clustered together, except a sham control from a 'chemical' model that was excluded from subsequent analysis.

Methylation array data were integrated with RNA sequencing data using the following criteria: (a) differentially methylated regions (DMRs) ($P < 0.01$); (b) all the CpGs in a functional methylation region are in the same direction, i.e., all hyper, or hypo-methylated; and (c) >50% of CpG sites in the region have delta beta >0.1. We identified 519 DMRs, corresponding to 81 genes that passed CPM filter (>1) in RNA-seq. Among them, 21 genes were differentially expressed (FDR < 0.05).

2.6. RNA sequencing

Genomic DNA and RNA were extracted using AllPrep DNA/RNA kit (Qiagen). Raw reads from RNA sequencing were assessed for quality using FastQC [23]. Adapter sequences were trimmed and low quality reads ($q < 20$) were filtered using cutadapt [24]. Reads were aligned to the human genome (GRCh37) using hisat2 [25]. Aligned SAM files were converted to BAM format using samtools [26]. Total aligned reads were quantified for each gene using featureCounts [27].

2.7. Quantitative RT-PCR

Quantitative RT-PCR was performed as described previously [6], using pre-designed TaqMan probe/primers (Applied Biosystems). 18S rRNA was used as internal control.

2.8. Analysis of methionine cycle metabolites

Concentrations of methionine, S-adenosylmethionine (SAM), S-adenosylhomocysteine (SAH), cystathionine, choline and betaine in cultured cells and mouse tissues were measured by liquid chromatography tandem mass spectrometry (LC-MS/MS) as previously described [28]. Total homocysteine (Hcy) and total cysteine (Cys) were also measured by LC-MS/MS as previously described [29].

2.9. Statistical analysis

Data were presented as mean ± SEM. Significance was determined using the Student's *t*-test.

3. Results and discussion

3.1. Effect of α-gal A deficiency on the methylation status of specific CpG sites in the AR gene promoter

To determine the potential role of Fabry disease on DNA methylation status, we examined whether manipulation of α-gal A activity and/or GSL levels lead to altered methylation levels in cultured cells. To this end, we employed two models – a 'genetic' model and a 'chemical' model (Fig. 1A). These models were generated using a Fabry patient-derived microvascular endothelial cell line (IMFE1) that exhibits both endothelial characteristics and Fabry phenotype [17]. In the 'genetic' model, IMFE1 cells were infected with a retroviral vector encoding wild type α-gal A to generate IMFE1(α-gal+), or infected with an 'empty' retroviral vector to generate IMFE1(mock) control. IMFE1(α-gal+) cells showed increased α-gal A activity and decreased lysosomal Gb_3 storage compared to IMFE1(mock) cells [6]. In the 'chemical' model, IMFE1 cells were treated with either 500 μM DGJ (a potent competitive inhibitor of α-gal A), or 0.5 μM GZ161 (an inhibitor of glucosylceramide synthase) for 12 days. IMFE1 harbors the R112H *GLA* mutation, and thus retains residual α-gal A activity (~15% of normal controls) [17]. The purpose of using DGJ in this experiment was to extinguish this residual activity and thereby exacerbate Gb_3 accumulation. Compared to sham treated IMFE1 cells, DGJ treatment resulted in markedly increased Gb_3 accumulation (Fig. 1B, C). Consistent with a previous study [30], GZ161 treatment led to significantly decreased Gb_3 relative to sham control

A

Cellular models	Effect of the treatments
Genetic model	
IMFE1(mock)	
IMFE1(α-gal+)	Overexpresses α-gal A
Chemical model	
IMFE1-sham	
IMFE1-DGJ treatment	Inhibits residual activity
IMFE1-GZ161 treatment	Inhibits GSLs synthesis

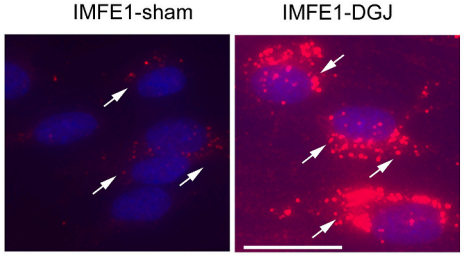

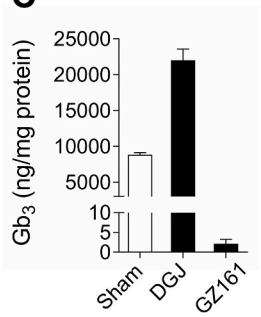

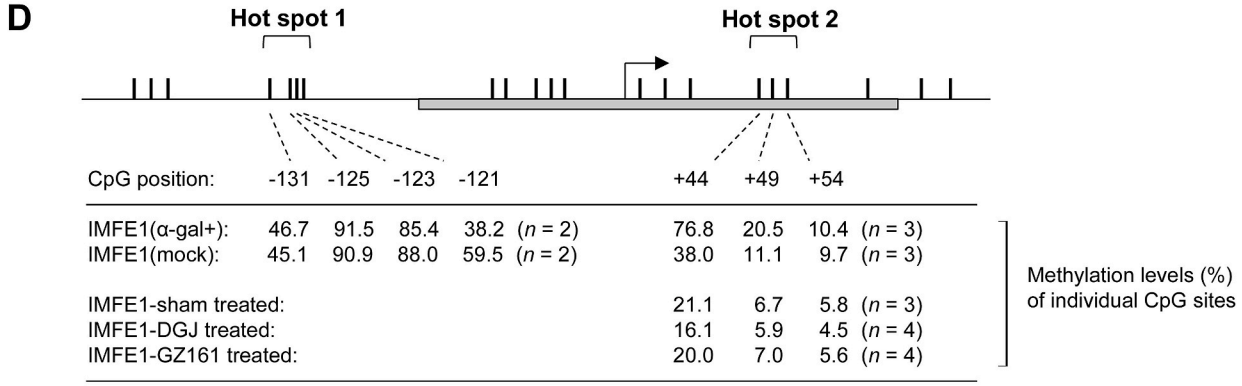

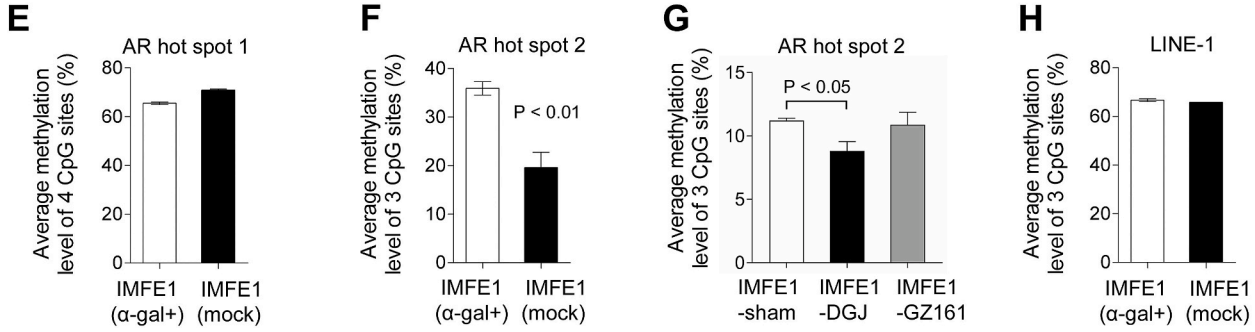

Fig. 1. Cell models and the effect of α-gal A deficiency in methylation of specific CpG sites in AR gene promoter.
(A) Summary of 'genetic' and 'chemical' cellular models used in this study. (B) Gb3 immunofluorescence staining demonstrating markedly increased lysosomal Gb3 storage in DGJ-treated IMFE1 cells compared to sham-treated control. Arrows indicate some of the Gb3 positive signals (red color). Scale bar, 25 μm. (C) Gb3 levels in sham-, DGJ-, or GZ161-treated IMFE1 cells measured by LC-MS/MS (n = 3). (D) Top: Map of 5′ region of human AR gene containing two 'hot spot' CpG regions. Each CpG is indicated by a vertical line. CpG nucleotide positions relative to transcription start site (indicated by right angle arrow), and the core-promoter region with a length of 150 bp that contains the elements essential for promoter activity (indicated by grey bar) are shown. Bottom: Methylation level (%) of individual CpG sites in two 'hot spots' measured by pyrosequencing. Data are means of biological replicates (n = 2–4). (E) Average methylation level of 4 CpG sites in AR hot spot 1 (n = 2). (F, G) Average methylation level of 3 CpG sites in AR hot spot 2 (n = 3–4). (H) Average methylation level of 3 CpG sites in LINE-1 (n = 2).

(Fig. 1C).

As the first step to test whether α-gal A deficiency and GSL accumulation affect DNA methylation, we analyzed methylation status of specific CpG sites in the androgen receptor (AR) gene as a marker. The AR gene was chosen because we had previously found that AR transcription is upregulated in Fabry disease [6]. Furthermore, the correlation between AR expression and DNA methylation has been well studied [31–33]. The 5′ region of human AR gene contains a ~ 3-kb CpG island with >80 CpG sites; among these, there are two specific CpG regions ('hot spots'), whose methylation is closely associated with AR gene silencing in prostate cancer cell lines [33]. These two hot spots (constituted by 4 and 3 CpG sites, respectively) are located near the transcription start site (Fig. 1D). We analyzed these CpG sites using bisulfite pyrosequencing, a sensitive and reliable method for quantitative determination of methylation [34]. In hot spot 1, the CpG site at nucleotide position −121 had a higher methylation level in IMFE1 (mock) than in IMFE1(α-gal+) cells, while the other three CpG sites (−123, −125, and − 131) remained unchanged (Fig. 1D). The average

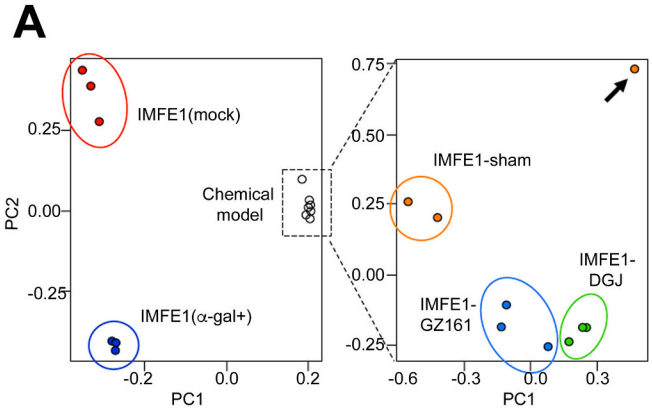

B

Cellular models	DMPs (P<0.05)	DMRs (P<0.05)
IMFE1(α-gal+) vs. IMFE1(mock)	236,881	73,983
IMFE1-DGJ vs. IMFE1-sham	66,454	10,849
IMFE1-GZ161 vs. IMFE1-sham	52,584	5,120

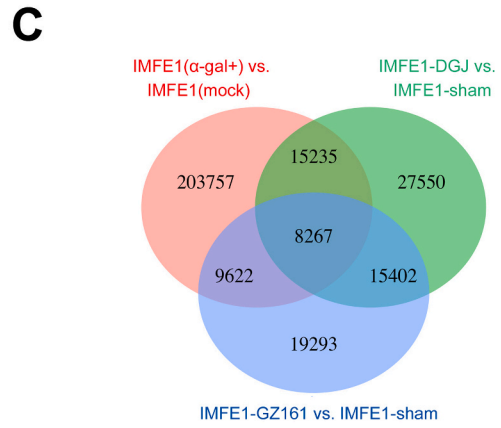

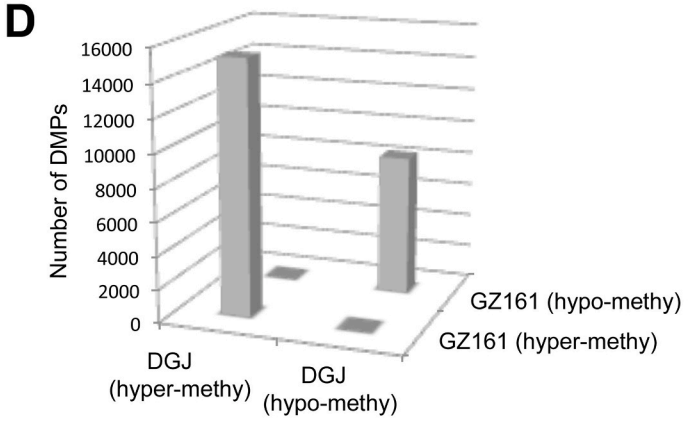

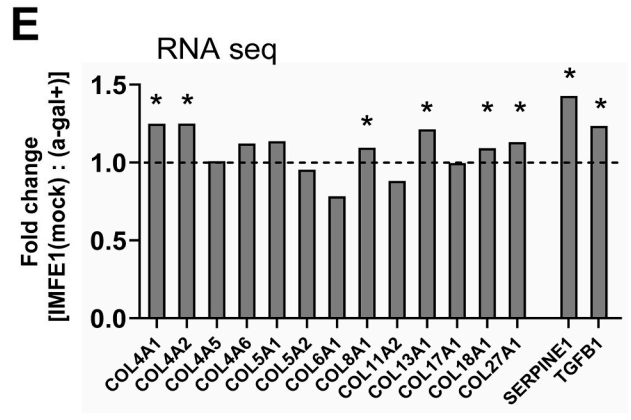

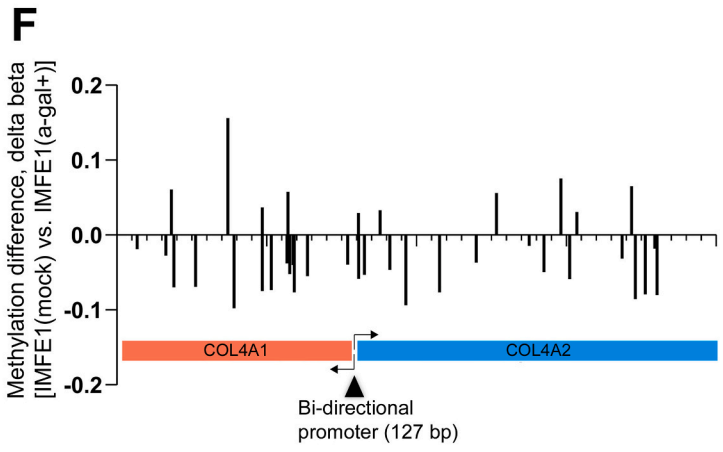

Fig. 2. DNA methylation array and RNA sequencing.
(**A**) Principal component analysis plot. Samples in each group ($n = 3$ per group) were clustered together, except a sham control from chemical model (arrow) that was excluded from the subsequent analysis. (**B**) Summary of numbers of DMPs and DMRs in each treatment group. (**C**) Venn diagram showing high proportion of common DMPs between different treatment groups. Numbers of DMPs were shown. (**D**) Majority of common DMPs between DGJ- and GZ161-treatment groups had the same direction of changes (hyper- or hypo-methylation) in both treatments. (**E**) RNA-seq results for collagen genes and profibrotic genes. Data were presented as fold-change [IMFE1(mock): IMFE1(α-gal+)]. *FDR < 0.05. (**F**) Map of DMPs (vertical lines) in COL4A1 and COL4A2 genes. Two arrows indicate transcription from a shared bi-directional promoter (shown as a triangle). Data were presented as methylation difference [delta beta values, IMFE1(mock) vs. IMFE1(α-gal+)]. Most DMPs in these two genes (13/17 and 14/20 probes, respectively) exhibited hypomethylation in IMFE1(mock).

methylation level of the 4 CpG sites in hot spot 1 was not substantially different between IMFE1(α-gal+) and IMFE1(mock) cells (Fig. 1E). In contrast, all three CpG sites in hot spot 2 (+44, +49, and + 54) had decreased methylation levels in IMFE1(mock) compared to IMFE1 (α-gal+) cells (Fig. 1D). The average methylation level of the 3 CpG sites in hot spot 2 was significantly lower in IMFE1(mock) compared to IMFE1(α-gal+) cells (Fig. 1F).

Because the methylation status was changed more significantly in hot spot 2 than hot spot 1, we only studied hot spot 2 in subsequent studies. Consistent with findings in the 'genetic' model, short-term treatment with DGJ led to decreased methylation in all three CpG sites, with the greatest change at +44, compared to sham control (Fig. 1D). The average methylation level of hot spot 2 was significantly decreased in DGJ-treated cells (Fig. 1G). The methylation levels of hot spot 2 were unchanged in GZ161-treated cells relative to sham control (Fig. 1D, G).

We analyzed long interspersed element-1 (LINE-1), the repetitive DNA elements that are randomly inserted throughout the human genome and thus are used as a marker for global methylation [35]. Methylation levels of three individual CpG sites in LINE-1 were not different between IMFE1(mock) and IMFE1(α-gal+) (Fig. 1H).

Collectively, these data suggested that changes in α-gal A activity and GSL levels in Fabry endothelial cells lead to altered DNA methylation in a highly CpG site-specific manner.

3.2. Genome-wide methylation changes in Fabry disease cellular models

We further tested the link between Fabry disease and DNA methylation in a genome-wide analysis. DNA methylation of a total 865,859 sites was analyzed in the 'genetic' and 'chemical' models using Infinium MethylationEPIC. After quality control filtering, 793,793 sites with reliable methylation data were used for further analysis. Principal component analysis showed that samples in each group clustered together (except one sample), and that treated cells were well separated from controls (Fig. 2A). We identified >230,000 differentially methylated probes (DMPs; $P < 0.05$) between IMFE1(α-gal+) and IMFE1 (mock), and > 50,000 DMPs in DGJ- or GZ161-treated cells versus sham-treated cells (Fig. 2B). Large numbers of differentially methylated regions (DMRs), which are composed of multiple DMPs, were also identified (Fig. 2B).

Of note, there was substantial overlapping in DMPs between different treatments. >23,000 DMPs were common between DGJ- and GZ161-treatments, which are ~40% of total numbers of DMPs in each group (Fig. 2C). Similarly, ~35% of DMPs in DGJ- or GZ161-treated groups overlapped with DMPs in the 'genetic' model (Fig. 2C). Because DGJ-treatment increases whereas GZ161 decreases substrate accumulation, one might expect that the direction of methylation changes (i.e., hyper- or hypomethylation relative to sham control) of the common DMPs in these two treatments should have an inverse relationship. On the contrary, the directions of methylation changes in these two treatments were highly consistent; 64.4% of common DMPs were hypermethylated in both treatments, and 35.4% were hypomethylated (Fig. 2D). Although detailed mechanisms of each treatment used to modulate DNA methylation can vary and will require further investigations, the high proportion of overlap in DMPs between different treatments suggests that these common DMPs might represent CpG sites whose methylation status has higher susceptibility to the changes in α-gal A activity and GSL levels. A total of 1044 genes were deduced from

Table 1
KEGG pathways with enrichment of genes that exhibit differential methylation in all 3 treatments.

Pathways	Number of genes	*P* value	Genes	Pop Hits	Pop Total	Fold Enrichment	Bonferroni	Benjamini	FDR
Adherens junction	9	0.0043	EGFR, PTPRM, PTPRF, ACTN4, SMAD4, LMO7, WASL, CTNNA1, CTNNA3	71	6879	3.419	0.6387	0.6387	5.497
cGMP-PKG signaling pathway	14	0.0054	SLC8A3, MYLK3, MRVI1, ATP1A4, NPR1, ATP2B2, MEF2D, PLCB3, ATF6B, GATA4, CACNA1F, CALM2, ADRA1D, OPRD1	158	6879	2.390	0.7185	0.4694	6.798
Calcium signaling pathway	14	0.0148	EGFR, SLC8A3, NOS1, PTGER3, MYLK3, GRIN2A, ATP2B2, PLCB3, PDE1A, RYR1, CACNA1F, ADRA1D, CALM2, CACNA1B	179	6879	2.109	0.9686	0.6847	17.499
Nicotine addiction	6	0.0151	GABRG3, GRIA2, GABRB2, GABRA6, GRIN2A, CACNA1B	40	6879	4.046	0.9702	0.5846	17.734
Gastric acid secretion	8	0.0176	PLCB3, MYLK3, ATP1A4, SLC4A2, CFTR, CA2, KCNQ1, CALM2	73	6879	2.956	0.9835	0.5603	20.405
Glutamatergic synapse	10	0.0246	DLGAP1, PLCB3, SLC1A3, GRIA2, GRIK1, GRM7, GRIN2A, HOMER1, SHANK2, GNG7	114	6879	2.366	0.9968	0.6173	27.395
Central carbon metabolism in cancer	7	0.0299	FGFR2, PKM, EGFR, NTRK3, FGFR3, NTRK1, SLC2A1	64	6879	2.950	0.9991	0.6337	32.329
Adrenergic signaling in cardiomyocytes	11	0.0311	ATP2B2, PLCB3, BCL2, ATF6B, ATP1A4, CACNA1F, CACNA2D3, KCNQ1, PPP2R2C, ADRA1D, CALM2	138	6879	2.150	0.9993	0.5987	33.349
Inositol phosphate metabolism	7	0.0463	INPP1, PLCB3, PIK3C2G, PLCH1, IPMK, MTMR7, INPP5A	71	6879	2.659	0.9999	0.7045	45.636
Regulation of actin cytoskeleton	14	0.0466	FGFR2, EGFR, FGFR3, ACTN4, DIAPH2, MYLK3, ITGA1, VAV2, ITGAX, CFL2, SCIN, MOS, WASL, FGD3	210	6879	1.798	0.9999	0.6682	45.815
Phosphatidylinositol signaling system	8	0.0696	INPP1, PLCB3, PIK3C2G, DGKG, IPMK, MTMR7, INPP5A, CALM2	98	6879	2.202	0.9999	0.7804	60.394
Retrograde endocannabinoid signaling	8	0.0790	PLCB3, GABRG3, GRIA2, GABRB2, GABRA6, CACNA1F, GNG7, CACNA1B	101	6879	2.136	0.9999	0.7951	65.243
Neuroactive ligand-receptor interaction	16	0.0863	AVPR2, GABRG3, PTGER3, GRIK1, GZMA, GABRB2, GABRA6, GRIN2A, CRHR1, GRIA2, GRM7, GALR2, CNR2, ADRA1D, OPRD1, GRID1	277	6879	1.558	0.9999	0.7990	68.602
Insulin secretion	7	0.0933	PLCB3, GIP, SLC2A1, ATF6B, ATP1A4, CACNA1F, RIMS2	85	6879	2.221	1	0.8015	71.563
Salivary secretion	7	0.0974	ATP2B2, PLCB3, NOS1, ATP1A4, SLC4A2, ADRA1D, CALM2	86	6879	2.195	1	0.7937	73.161

CpG sites that are differentially methylated in all three treatments ($P < 0.01$). From these genes, KEGG pathway analysis [36,37] identified 15 relevant signaling pathways (Table 1). It is possible that these genes and pathways are vulnerable to aberrant methylation status in Fabry disease.

Overall methylation levels in different CpG regions (e.g., island) or gene regions (e.g., TSS-200) were similar between treated and control cells (**Supplementary Fig. 1A-D**). DMPs were evenly distributed across the chromosomes (**Supplementary Fig. 1E**). Distribution of DMPs that were common in all three treatments in different gene, and CpG regions, and chromosomes was proportional to that of all 793,793 probes (**Supplementary Fig. 1F**). These findings suggested that, unlike in cancers, where the methylation changes preferentially occur in specific regions (CpG island shores) [38], the differentially methylated CpGs in Fabry disease cellular models were relatively evenly distributed in various gene regions and chromosomes, and did not cause global changes in methylation level.

3.3. Differential mRNA expression and methylation in Fabry cellular models

We analyzed the transcriptome in the 'genetic' model using RNA-seq. We identified >3000 differentially expressed genes between IMFE1 (α-gal+) and IMFE1(mock) cells (FDR < 0.05; **Supplementary Table 1**) and 85 relevant signaling pathways (**Supplementary Table 2**). By integrating the methylation array and RNA-seq data (details, see **Materials and Methods**), we identified 21 genes that exhibited both differential DNA methylated regions and gene expression (**Supplementary Table 3**).

Among the signaling pathways identified from RNA-seq (**Supplementary Table 2**), we took specific interest in extracellular matrix-related pathways, such as those involved in focal adhesion, and ECM-receptor interaction. Fibrosis is a prominent pathological feature in Fabry disease [39]. We found that 6 out of 13 collagen genes in the RNA-seq results were differentially expressed (FDR < 0.05), and they were exclusively upregulated in IMFE1(mock) relative to IMFE1(α-gal+) cells (Fig. 2E). SERPINE1, which encodes profibrotic protein plasminogen activator inhibitor-1 (PAI-1) [40], was also upregulated (~43%) in IMFE1(mock) cells (Fig. 2E). TGF-β1, which is a key mediator of fibrotic process [41] and induces expression of several collagens and PAI-1 [42,43], was significantly upregulated in IMFE1(mock) cells (Fig. 2E). These gene changes are consistent with the enhanced fibrosis in Fabry disease and also with previous laboratory findings, e.g., upregulated SERPINE1 in Fabry mouse penis [7], and enhanced TGF-β1 immunostaining in Fabry patient's kidney biopsies [44].

Among these genes, COL4A1 and COL4A2 exhibited significant changes in methylation status. Most DMPs in these two genes (13/17 and 14/20 probes, respectively) exhibited hypomethylation in IMFE1 (mock) cells (Fig. 2F). COL4A1 and COL4A2 genes are arranged head-to-head on opposite strands of chromosome 13, and are separated by a shared, bidirectional promoter [45] (Fig. 2F). This short promoter (127 base pairs) does not show significant transcriptional activity, and requires regulatory elements present on distant portions of both genes [45,46]. The coordinated expression of both genes is necessary for function of the protein. In agreement with this, both genes were upregulated in IMFE1(mock) cells to the same extent (25%) (Fig. 2E). Earlier studies suggested that DNA demethylation correlated with induction of COL4A1/2 expression during differentiation of F9 teratocarcinoma cells [47]. Our data suggests that Fabry disease is associated with decreased methylation of both COL4A1 and COL4A2 genes, and this may contribute to upregulated transcription of these genes. Peptides encoded by COL4A1 and COL4A2 form collagen type IV α1α1α2 heterotrimer, which is the major component of basement membranes. This protein is involved in a number of physiological and pathophysiological conditions, including angiogenesis and brain small vessel diseases [48]. It is possible that increased expression of COL4A1/2 contributes to the development of vasculopathy in Fabry disease.

3.4. Potential basis of altered DNA methylation in Fabry disease

To study the potential basis of the altered DNA methylation, we tested whether levels of SAM, the methyl donor for DNA methylation, and other methionine cycle metabolites are changed in Fabry disease. Relative to IMFE1(α-gal+) cells, the level of methionine was significantly increased and cystathionine was decreased in IMFE1(mock) cells (Fig. 3A). We also analyzed kidney tissues from Fabry and WT mice. Consistent with the findings in the cellular models, the methionine level was significantly increased in Fabry mouse kidneys compared to WT mice (Fig. 3B). SAH in Fabry mice trended towards a higher level ($P = 0.053$). There was a strong positive correlation between levels of methionine and cystathionine in both WT and Fabry mouse kidney tissues (Fig. 3C, left). Methionine also positively correlated with SAM/SAH ratio in WT mice kidneys, but not in Fabry mouse kidneys (Fig. 3C, right).

Methionine cycle metabolism plays pivotal roles in the methylation process [49]. A number of animal studies using dietary approaches - either restricting or supplementing methionine or its metabolites betaine and choline - demonstrated the role of these compounds in modifying DNA methylation [50,51]. However, an increased methionine level was not always associated with increased SAM. For instance, 6 weeks of methionine supplementation in rats caused increased renal concentration of SAH, but no change in SAM and SAM/SAH [52]. Moreover, it was suggested that the effect of methionine supplementation on DNA methylation might be gene-specific, rather than global [53]. Collectively, our findings suggest that the disturbed methionine cycle could be part of the basis for the altered DNA methylation patterns in Fabry disease.

From the RNA-seq results, we summarized the expression of major enzymes that regulate methionine metabolism and the methylation/demethylation processes [49,54] (Fig. 3D, E). Methionine adenosyltransferase (MAT) 2B was downregulated in IMFE1(mock) compared to IMFE1(α-gal+) cells (Fig. 3E). MAT catalyzes the synthesis of SAM from methionine (Fig. 3D). In MATII isoenzyme, the regulatory subunit MATβ (encoded by MAT2B) interacts with catalytic subunit MATα2 (encoded by MAT2A) to form a heterotetramer [55]. MATβ increases the activity of MATII complex by lowering its K_m for the substrate, methionine [56]. Therefore, downregulation of MAT2B may contribute to the increased methionine in Fabry disease cells and tissues. However, it is not clear whether MAT2B expression change is a reason for increased methionine, or is a secondary change resulting from altered methylation. Other potential explanations for the imbalanced methionine metabolism may relate to oxidative stress and dysregulated nitric oxide (NO) pathway in Fabry disease [57–59]. NO inhibits the activity of methionine synthase, the enzyme responsible for regeneration of methionine from homocysteine [60]. It is possible that decreased NO production in Fabry disease due to NO synthase uncoupling [58,59] may lead to increased methionine synthase activity.

In addition, both RNA-seq and quantitative RT-PCR revealed that ten-eleven translocation 1 (TET1), the enzyme involved in DNA demethylation [54,61], was significantly downregulated (~40%) in IMFE1 (mock) (Fig. 3E, F), suggesting that TET1 may also be involved in the altered DNA methylation homeostasis in Fabry disease.

4. Conclusions

By combining unique cellular models based on Fabry patient-derived endothelial cells that are disease-relevant, and loci-specific pyrosequencing and genome-wide arrays, the present study demonstrated that abnormal glycolipid metabolism in Fabry disease may affect DNA methylation homeostasis. The dysregulated methylation was associated with altered methionine metabolism. These findings provide new insights into the pathogenic mechanism of this complex disease. DNA methylation, together with other epigenetic mechanisms, may also play a role in the phenotypic heterogeneity noted in Fabry and other LSD

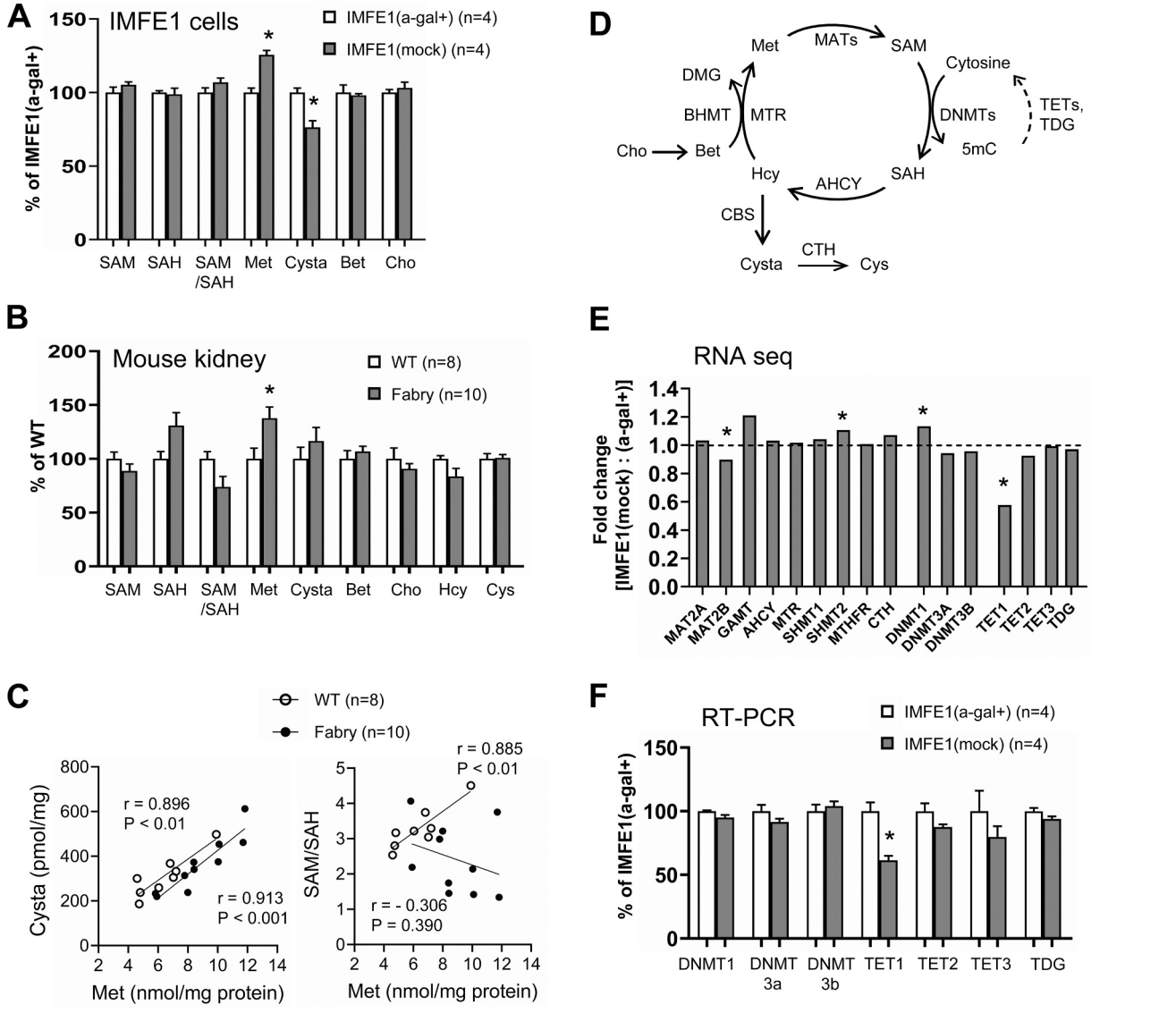

Fig. 3. Methionine cycle metabolism and DNA methylation.
(A, B) Methionine cycle metabolites in IMFE1 cells (A) and 6-month-old male mouse kidneys (B). *P < 0.05. Data were presented as % of levels in normal controls. Met, methionine; SAM, S-adenosylmethionine; SAH, S-adenosylhomocysteine; Cysta, cystathionine, Bet, betaine; Cho, choline; Hcy, homocysteine (total); Cys, cysteine (total). (C) Correlations between methionine levels and cystathionine (left), and SAM/SAH ratio (right) in mouse kidneys. (D) Schema of methionine cycle and DNA methylation/demethylation reactions. The major enzymes involved in these reactions were shown. MAT, methionine adenosyltransferase; GAMT, guanidinoacetate methyltransferase; GNMT, glycine N-methyltransferase; AHCY, s-adenosylhomocysteine hydrolase; BHMT, betaine-homocysteine methyltransferase; MTR, methionine synthase; SHMT, serine hydroxymethyltransferase; MTHFR, methylenetetrahydrofolate reductase; CBS, cystathionine β-synthase; CTH, cystathionine γ-lyase; GATM, L-arginine/glycine amidinotransferase; DNMT, DNA methyltransferase; TET, ten-eleven translocation, TDG, thymine-DNA glycosylase; DMG, dimethylglycine; 5mC, 5-methylcytosine. (E) Transcription levels (RNA-Seq data) of major enzymes that are involved in methionine cycle and DNA methylation/demethylation reactions. Data were presented as fold-change [IMFE1(mock): IMFE1(α-gal+)]. *FDR < 0.05. (F) mRNA levels of DNA methylation/demethylation related genes measured by quantitative RT-PCR. *P < 0.05.

patients.

In addition, from the perspective of therapeutics, data from α-gal A overexpression and GZ161 treatment in the cells may provide useful information for gene therapy and substrate reduction therapy, respectively. Both approaches are under active investigation currently as new therapies for Fabry patients [62–64]. As shown from the RNA-seq and methylation array results, these treatments change the expression of numerous genes as well as methylation status throughout the genome. Our results may serve as a database for investigating potential clinical biomarkers for these therapies.

Supplementary data to this article can be found online at https://doi.org/10.1016/j.ymgmr.2022.100919.

Declaration of Competing Interest

None.

Data availability

Data will be made available on request.

Acknowledgements

This work was supported by Baylor Scott & White Research Institute Foundation.

References

[1] R. Brady, A.E. Gal, R.M. Bradley, E. Martensson, A.L. Warshaw, L. Laster, Enzymatic defect in Fabry disease: ceramide trihexosidase deficiency, N. Engl. J. Med. 276 (1967) 1163–1167.

[2] R.J. Desnick, Y.A. Ioannou, C.M. Eng, in: C.R. Scriver, A.L. Beaudet, W.S. Sly, D. Valle (Eds.), In The Metabolic and Molecular Bases of Inherited Disease, McGraw-Hill, New York, 2001, pp. 3733–3774.

[3] R. Schiffmann, Fabry disease, Pharmacol. Ther. 122 (2009) 65–77.

[4] D.F. Moore, M.P. Gelderman, P.A. Ferreira, S.R. Fuhrmann, H. Yi, A. Elkahloun, L. M. Lix, R.O. Brady, R. Schiffmann, E. Goldin, Genomic abnormalities of the murine model of Fabry disease after disease-related perturbation, a systems biology approach, Proc. Natl. Acad. Sci. U. S. A. 104 (2007) 8065–8070.

[5] D.F. Moore, O.V. Krokhin, R.C. Beavis, M. Ries, C. Robinson, E. Goldin, R.O. Brady, J.A. Wilkins, R. Schiffmann, Proteomics of specific treatment-related alterations in Fabry disease: a strategy to identify biological abnormalities, Proc. Natl. Acad. Sci. U. S. A. 104 (2007) 2873–2878.

[6] J.S. Shen, X.L. Meng, M. Wight-Carter, T.S. Day, S.C. Goetsch, S. Forni, J. W. Schneider, Z.P. Liu, R. Schiffmann, Blocking hyperactive androgen receptor signaling ameliorates cardiac and renal hypertrophy in Fabry mice, Hum. Mol. Genet. 24 (2015) 3181–3191.

[7] X.L. Meng, E. Arning, M. Wight-Carter, T.S. Day, S. Jabbarzadeh-Tabrizi, S. Chen, R.J. Ziegler, T. Bottiglieri, J.W. Schneider, S.H. Cheng, et al., Priapism in a Fabry disease mouse model is associated with upregulated penile nNOS and eNOS expression, J. Inherit. Metab. Dis. 41 (2018) 231–238.

[8] Z. Hollander, D.L. Dai, B.N. Putko, H. Yogasundaram, J.E. Wilson-McManus, R. B. Thompson, A. Khan, M.L. West, B.M. McManus, G.Y. Oudit, Gender-specific plasma proteomic biomarkers in patients with Anderson-Fabry disease, Eur. J. Heart Fail. 17 (2015) 291–300.

[9] G.G. Slaats, F. Braun, M. Hoehne, L.E. Frech, L. Blomberg, T. Benzing, B. Schermer, M.M. Rinschen, C.E. Kurschat, Urine-derived cells: a promising diagnostic tool in Fabry disease patients, Sci. Rep. 8 (2018) 11042.

[10] A. Portela, M. Esteller, Epigenetic modifications and human disease, Nat. Biotechnol. 28 (2010) 1057–1068.

[11] L. Echevarria, K. Benistan, A. Toussaint, O. Dubourg, A.A. Hagege, D. Eladari, F. Jabbour, C. Beldjord, P. De Mazancourt, D.P. Germain, X-chromosome inactivation in female patients with Fabry disease, Clin. Genet. 89 (2016) 44–54.

[12] R. Rossanti, K. Nozu, A. Fukunaga, C. Nagano, T. Horinouchi, T. Yamamura, N. Sakakibara, S. Minamikawa, S. Ishiko, Y. Aoto, et al., X-chromosome inactivation patterns in females with Fabry disease examined by both ultra-deep RNA sequencing and methylation-dependent assay, Clin. Exp. Nephrol. 25 (2021) 1224–1230.

[13] G. De Riso, M. Cuomo, T. Di Risi, R.D. Monica, M. Buonaiuto, D. Costabile, A. Pisani, S. Cocozza, L. Chiariotti, Ultra-deep DNA methylation analysis of X-linked genes: GLA and AR as model genes, Genes (Basel) 11 (2020) 620.

[14] M.A. Hossain, C. Wu, H. Yanagisawa, T. Miyajima, K. Akiyama, Y. Eto, Future clinical and biochemical predictions of Fabry disease in females by methylation studies of the GLA gene, Mol. Geneti. Metabol. Rep. 20 (2019), 100497.

[15] M.A. Hossain, H. Yanagisawa, T. Miyajima, C. Wu, A. Takamura, K. Akiyama, R. Itagaki, K. Eto, T. Iwamoto, T. Yokoi, et al., The severe clinical phenotype for a heterozygous Fabry female patient correlates to the methylation of non-mutated allele associated with chromosome 10q26 deletion syndrome, Mol. Genet. Metab. 120 (2017) 173–179.

[16] T. Di Risi, R. Vinciguerra, M. Cuomo, R.D. Monica, E. Riccio, S. Cocozza, M. Imbriaco, G. Duro, A. Pisani, L. Chiariotti, DNA methylation impact on Fabry disease, Clin. Epigenetics 13 (2021) 24.

[17] J.S. Shen, X.L. Meng, R. Schiffmann, R.O. Brady, C.R. Kaneski, Establishment and characterization of Fabry disease endothelial cells with an extended lifespan, Mol. Genet. Metab. 92 (2007) 137–144.

[18] M.A. Cabrera-Salazar, M. Deriso, S.D. Bercury, L. Li, J.T. Lydon, W. Weber, N. Pande, M.A. Cromwell, D. Copeland, J. Leonard, et al., Systemic delivery of a glucosylceramide synthase inhibitor reduces CNS substrates and increases lifespan in a mouse model of type 2 Gaucher disease, PLoS One 7 (2012), e43310.

[19] M.J. Aryee, A.E. Jaffe, H. Corrada-Bravo, C. Ladd-Acosta, A.P. Feinberg, K. D. Hansen, R.A. Irizarry, Minfi: a flexible and comprehensive Bioconductor package for the analysis of Infinium DNA methylation microarrays, Bioinformatics 30 (2014) 1363–1369.

[20] K.D. Hansen, IlluminaHumanMethylationEPICanno.ilm10b4.hg19: Annotation for Illumina's EPIC methylation arrays, in: R package version 0.6.0, 2017. *https://bitbucket.com/kasperdanielhansen/Illumina_EPIC*.

[21] M.E. Ritchie, B. Phipson, D. Wu, Y. Hu, C.W. Law, W. Shi, G.K. Smyth, Limma powers differential expression analyses for RNA-sequencing and microarray studies, Nucleic Acids Res. 43 (2015), e47.

[22] T.J. Peters, M.J. Buckley, A.L. Statham, R. Pidsley, K. Samaras, R.V. Lord, S. J. Clark, P.L. Molloy, De novo identification of differentially methylated regions in the human genome, Epigenetics Chromatin 8 (2015) 6.

[23] S. Andrews, FastQC: a quality control tool for high throughput sequence data. http://www.bioinformatics.babraham.ac.uk/projects/fastqc, 2010.

[24] M. Martin, Cutadapt removes adapter sequences from high-throughput sequencing reads, EMBnet.journal (2011) 17.1.

[25] D. Kim, B. Langmead, S.L. Salzberg, HISAT: a fast spliced aligner with low memory requirements, Nat. Methods 12 (2015) 357–360.

[26] H. Li, B. Handsaker, A. Wysoker, T. Fennell, J. Ruan, N. Homer, G. Marth, G. Abecasis, R. Durbin, The sequence alignment/map format and SAMtools, Bioinformatics 25 (2009) 2078–2079.

[27] Y. Liao, G.K. Smyth, W. Shi, featureCounts: an efficient general purpose program for assigning sequence reads to genomic features, Bioinformatics 30 (2014) 923–930.

[28] M. Rooney, T. Bottiglieri, B. Wasek-Patterson, A. McMahon, C.F. Hughes, A. McCann, G. Horigan, J.J. Strain, H. McNulty, M. Ward, Impact of the MTHFR C677T polymorphism on one-carbon metabolites: evidence from a randomised trial of riboflavin supplementation, Biochimie 173 (2020) 91–99.

[29] V. Ducros, H. Belva-Besnet, B. Casetta, A. Favier, A robust liquid chromatography tandem mass spectrometry method for total plasma homocysteine determination in clinical practice, Clin. Chem. Lab. Med. 44 (2006) 987–990.

[30] J.S. Shen, E. Arning, M.L. West, T.S. Day, S. Chen, X.L. Meng, S. Forni, N. McNeill, O. Goker-Alpan, X. Wang, et al., Tetrahydrobiopterin deficiency in the pathogenesis of Fabry disease, Hum. Mol. Genet. 26 (2017) 1182–1192.

[31] K.K. Takane, M.J. McPhaul, Functional analysis of the human androgen receptor promoter, Mol. Cell. Endocrinol. 119 (1996) 83–93.

[32] T. Nakayama, M. Watanabe, H. Suzuki, M. Toyota, N. Sekita, Y. Hirokawa, A. Mizokami, H. Ito, R. Yatani, T. Shiraishi, Epigenetic regulation of androgen receptor gene expression in human prostate cancers, Lab. Investig. 80 (2000) 1789–1796.

[33] H. Kinoshita, Y. Shi, C. Sandefur, L.F. Meisner, C. Chang, A. Choon, C.R. Reznikoff, G.S. Bova, A. Friedl, D.F. Jarrard, Methylation of the androgen receptor minimal promoter silences transcription in human prostate cancer, Cancer Res. 60 (2000) 3623–3630.

[34] C. Delaney, S.K. Garg, R. Yung, Analysis of DNA methylation by pyrosequencing, Methods Mol. Biol. 1343 (2015) 249–264.

[35] A.S. Yang, M.R. Estecio, K. Doshi, Y. Kondo, E.H. Tajara, J.P. Issa, A simple method for estimating global DNA methylation using bisulfite PCR of repetitive DNA elements, Nucleic Acids Res. 32 (2004), e38.

[36] M. Kanehisa, S. Goto, KEGG: Kyoto encyclopedia of genes and genomes, Nucleic Acids Res. 28 (2000) 27–30.

[37] D.W. Huang, B.T. Sherman, R.A. Lempicki, Systematic and integrative analysis of large gene lists using DAVID bioinformatics resources, Nat. Protoc. 4 (2009) 44–57.

[38] R.A. Irizarry, C. Ladd-Acosta, B. Wen, Z. Wu, C. Montano, P. Onyango, H. Cui, K. Gabo, M. Rongione, M. Webster, et al., The human colon cancer methylome shows similar hypo- and hypermethylation at conserved tissue-specific CpG island shores, Nat. Genet. 41 (2009) 178–186.

[39] F. Weidemann, M.D. Sanchez-Nino, J. Politei, J.P. Oliveira, C. Wanner, D. G. Warnock, A. Ortiz, Fibrosis: a key feature of Fabry disease with potential therapeutic implications, Orphanet J. Rare Dis. 8 (2013) 116.

[40] A.K. Ghosh, D.E. Vaughan, PAI-1 in tissue fibrosis, J. Cell. Physiol. 227 (2012) 493–507.

[41] A. Biernacka, M. Dobaczewski, N.G. Frangogiannis, TGF-beta signaling in fibrosis, Growth Factors 29 (2011) 196–202.

[42] F. Verrecchia, M.L. Chu, A. Mauviel, Identification of novel TGF-beta /Smad gene targets in dermal fibroblasts using a combined cDNA microarray/promoter transactivation approach, J. Biol. Chem. 276 (2001) 17058–17062.

[43] S. Dennler, S. Itoh, D. Vivien, P. ten Dijke, S. Huet, J.M. Gauthier, Direct binding of Smad3 and Smad4 to critical TGF beta-inducible elements in the promoter of human plasminogen activator inhibitor-type 1 gene, EMBO J. 17 (1998) 3091–3100.

[44] P.A. Rozenfeld, M. de Los Angeles Bolla, P. Quieto, A. Pisani, S. Feriozzi, P. Neuman, C. Bondar, Pathogenesis of Fabry nephropathy: the pathways leading to fibrosis, Mol. Genet. Metab. 129 (2020) 132–141.

[45] E. Poschl, R. Pollner, K. Kuhn, The genes for the alpha 1(IV) and alpha 2(IV) chains of human basement membrane collagen type IV are arranged head-to-head and separated by a bidirectional promoter of unique structure, EMBO J. 7 (1988) 2687–2695.

[46] A. Haniel, U. Welge-Lussen, K. Kuhn, E. Poschl, Identification and characterization of a novel transcriptional silencer in the human collagen type IV gene COL4A2, J. Biol. Chem. 270 (1995) 11209–11215.

[47] P.D. Burbelo, S. Horikoshi, Y. Yamada, DNA methylation and collagen IV gene expression in F9 teratocarcinoma cells, J. Biol. Chem. 265 (1990) 4839–4843.

[48] D.S. Kuo, C. Labelle-Dumais, D.B. Gould, COL4A1 and COL4A2 mutations and disease: insights into pathogenic mechanisms and potential therapeutic targets, Hum. Mol. Genet. 21 (2012) R97–110.

[49] C.L. Ulrey, L. Liu, L.G. Andrews, T.O. Tollefsbol, The impact of metabolism on DNA methylation, Hum. Mol. Genet. 14 (2005). Spec No 1. R139-147.

[50] N. Zhang, Role of methionine on epigenetic modification of DNA methylation and gene expression in animals, Animal Nutrition 4 (2018) 11–16.

[51] A.M. Mahmoud, M.M. Ali, Methyl donor micronutrients that modify DNA methylation and cancer outcome, Nutrients 11 (2019).

[52] C.L. Amaral, B. Bueno Rde, R.V. Burim, R.H. Queiroz, L. Bianchi Mde, L. M. Antunes, The effects of dietary supplementation of methionine on genomic stability and p53 gene promoter methylation in rats, Mutat. Res. 722 (2011) 78–83.

[53] E. Dong, R.C. Agis-Balboa, M.V. Simonini, D.R. Grayson, E. Costa, A. Guidotti, Reelin and glutamic acid decarboxylase67 promoter remodeling in an epigenetic methionine-induced mouse model of schizophrenia, Proc. Natl. Acad. Sci. U. S. A. 102 (2005) 12578–12583.

[54] N. Bhutani, D.M. Burns, H.M. Blau, DNA demethylation dynamics, Cell 146 (2011) 866–872.

[55] K. Ramani, S.C. Lu, Methionine adenosyltransferases in liver health and diseases, Liver Res. 1 (2017) 103–111.

[56] A.B. Halim, L. LeGros, A. Geller, M. Kotb, Expression and functional interaction of the catalytic and regulatory subunits of human methionine adenosyltransferase in mammalian cells, J. Biol. Chem. 274 (1999) 29720–29725.

[57] D.F. Moore, L.T. Scott, M.T. Gladwin, G. Altarescu, C. Kaneski, K. Suzuki, M. Pease-Fye, R. Ferri, R.O. Brady, P. Herscovitch, et al., Regional cerebral hyperperfusion and nitric oxide pathway dysregulation in Fabry disease: reversal by enzyme replacement therapy, Circulation 104 (2001) 1506–1512.
[58] L. Shu, J.L. Park, J. Byun, S. Pennathur, J. Kollmeyer, J.A. Shayman, Decreased nitric oxide bioavailability in a mouse model of Fabry disease, J. Am. Soc. Nephrol. 20 (2009) 1975–1985.
[59] J.J. Kang, L. Shu, J.L. Park, J.A. Shayman, P.F. Bodary, Endothelial nitric oxide synthase uncoupling and microvascular dysfunction in the mesentery of mice deficient in alpha-galactosidase A, Am. J. Physiol. Gastrointest. Liver Physiol. 306 (2014) G140–G146.
[60] I.O. Danishpajooh, T. Gudi, Y. Chen, V.G. Kharitonov, V.S. Sharma, G.R. Boss, Nitric oxide inhibits methionine synthase activity in vivo and disrupts carbon flow through the folate pathway, J. Biol. Chem. 276 (2001) 27296–27303.
[61] R.M. Kohli, Y. Zhang, TET enzymes, TDG and the dynamics of DNA demethylation, Nature 502 (2013) 472–479.
[62] J. Huang, A. Khan, B.C. Au, D.L. Barber, L. Lopez-Vasquez, N.L. Prokopishyn, M. Boutin, M. Rothe, J.W. Rip, M. Abaoui, et al., Lentivector iterations and pre-clinical scale-up/toxicity testing: targeting mobilized CD34(+) cells for correction of Fabry disease, Mol. Therapy. Methods Clin. Develop. 5 (2017) 241–258.
[63] K.M. Ashe, E. Budman, D.S. Bangari, C.S. Siegel, J.B. Nietupski, B. Wang, R. J. Desnick, R.K. Scheule, J.P. Leonard, S.H. Cheng, et al., Efficacy of enzyme and substrate reduction therapy with a novel antagonist of glucosylceramide synthase for Fabry disease, Mol. Med. 21 (2015) 389–399.
[64] R.W.D. Welford, A. Muhlemann, M. Garzotti, V. Rickert, P.M.A. Groenen, O. Morand, N. Uceyler, M.R. Probst, Glucosylceramide synthase inhibition with lucerastat lowers globotriaosylceramide and lysosome staining in cultured fibroblasts from Fabry patients with different mutation types, Hum. Mol. Genet. 27 (2018) 3392–3403.